GRIFFITH UNIVERSITY

Unsaturated flow through a spherical inclusion

Author

Warrick, A., Knight, John

Published

2004

Journal Title

Water Resources Research

Version

Version of Record (VoR)

DOI

10.1029/2003WR002890

Rights statement

© 2004 American Geophysical Union. The attached file is reproduced here in accordance with the copyright policy of the publisher. Please refer to the journal's website for access to the definitive, published version.

Downloaded from

http://hdl.handle.net/10072/5207

Griffith Research Online

https://research-repository.griffith.edu.au

Unsaturated flow through a spherical inclusion

A. W. Warrick

Department of Soil, Water, and Environmental Sciences, University of Arizona, Tucson, Arizona, USA

J. H. Knight

Centre for Mathematics and its Applications, Mathematical Sciences Institute, Australian National University, Canberra, ACT, Australia

Received 18 November 2003; revised 10 February 2004; accepted 23 February 2004; published 4 May 2004.

[1] Unsaturated flow is considered through a spherical inclusion. The hydraulic conductivity is of the form $K_i\exp(\alpha h)$, where the saturated conductivity K_i is different in the main flow regime, the inclusion α is a constant in the entire flow domain, and h is the pressure head. The solution technique is analogous to that used by the authors previously to analyze flow through circular inclusions for two-dimensional flow by reducing Richards' equation to the Helmholtz equation and applying the analytic element method. Comparisons show differences between the two-dimensional case (circles) and three-dimensional case (spheres) in terms of flow enhancement and exclusion through the inclusions. When the inclusion permeability is less than the background conductivity, a lesser fraction of flow occurs through the three-dimensional case than for the two-dimensional case; conversely, when the permeability is higher within the inclusion, there is a higher enhancement of flow through that region in the case of the three-dimensional inclusion. *INDEX TERMS:* 1866 Hydrology: Soil moisture; 1875 Hydrology: Unsaturated zone; 1829 Hydrology: Groundwater hydrology; *KEYWORDS:* analytic element, Gardner soil, heterogeneity, soil moisture, unsaturated zone

Citation: Warrick, A. W., and J. H. Knight (2004), Unsaturated flow through a spherical inclusion, *Water Resour. Res.*, *40*, W05101, doi:10.1029/2003WR002890.

1. Introduction

[2] Earlier we analyzed the unsaturated flow through circular inclusions within a two-dimensional system [*Warrick and Knight*, 2002]. Results were consistent with early work by *Philip et al.* [1989] which were for fully impervious inclusions relevant to descriptions of flow in regions proximate to macropores, tunnels, cavities, and around underground obstacles such as stones or structures. In that paper, it was pointed out that the analytic element method had also been applied earlier to saturated flow examples, including those for large number of spheroidal inhomogeneities (in a three-dimensional flow regime) *Janković and Barnes* [1999]. The result was a detailed picture of the flow domain which is sufficient to enable particle tracking or whatever might be of interest.

[3] The objective of the present study is to apply the analytic element method of *Janković and Barnes* [1999] to the unsaturated case for a spherical inclusion in a three-dimensional flow domain. The *Gardner* [1958] model for unsaturated flow is used, which results in a linear equation for the matric flux potential. It is assumed that the surrounding soil and the inclusion have the same value of the capillary length parameter but different saturated hydraulic conductivities. This reduces the problem to a solution of the Helmholtz equation and, initially, follows the direction of *Knight et al.* [1989] for a spherical inclusion which is totally impervious. However, when the inclusion is permeable, it is necessary to apply the analytic element method.

2. Theory

[4] Consider the spherical inclusion of radius r_1 centered at the origin in Figure 1a. The saturated hydraulic conductively is K_1, and the unsaturated hydraulic conductivity is for a Gardner soil of the form $K = K_1 exp(\alpha h)$. The inclusion is embedded within a larger flow region described by $K = K_0 exp(\alpha h)$. The background flow is characterized by a pressure head $h = h_0 < 0$ and a vertical flow rate of $K_0 exp(\alpha h_0)$ at large distances from the sphere. The polar coordinate and Cartesian coordinates are related by $\rho^2 = x^2 + y^2$. The flow rate everywhere is given by

$$\vec{J}_w = -K_i(\nabla\phi + \alpha\phi\nabla z) \tag{1}$$

with the matric flux potential equal to

$$K_i\phi = \frac{K_i \exp(\alpha h)}{\alpha} \tag{2}$$

and with $i = 0, 1$. The first part of equation (1) is flow due to pressure difference and the second part is due to gravity. For these definitions, Richards' equation becomes

$$\nabla^2\phi + \alpha\frac{\partial\phi}{\partial z} = 0 \tag{3}$$

(note that ϕ does not contain K_1 and z is positive in the upward direction).

Copyright 2004 by the American Geophysical Union.
0043-1397/04/2003WR002890

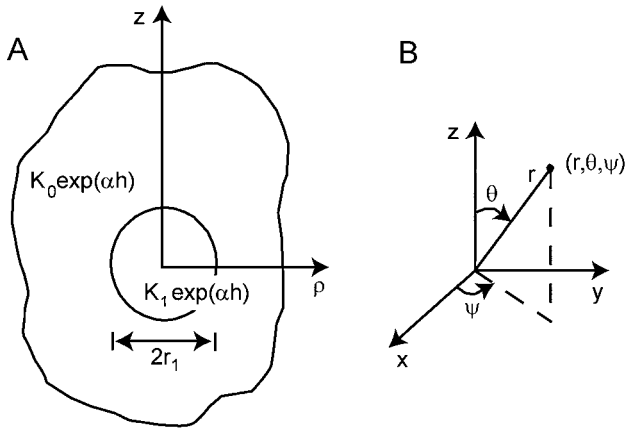

Figure 1. (a) Spherical inclusion and (b) spherical coordinate system.

[5] Without loss of generality, we introduce the Helmholtz function H with

$$H = \left(\frac{\phi}{\phi_0} - 1\right) \exp(0.5\alpha z) \tag{4}$$

The value of $\phi_0 = \exp(\alpha h_0) / \alpha$ is the limiting value of ϕ at large distances from the inclusion. Note that for background regions ϕ is ϕ_0 and H is 0. As shown by *Knight et al.* [1989], H satisfies the Helmholtz equation

$$\nabla^2 H + \chi^2 H = 0 \tag{5}$$

where

$$\chi^2 = -0.25\alpha^2 \tag{6}$$

[6] The solution of H may be taken of a separable form [*Moon and Spencer*, 1961, p. 27]

$$H = \sum_{n=0}^{\infty} R_n(r)\Theta_n(\theta) \tag{7}$$

where r is the spherical radial coordinate ($r^2 = x^2 + y^2 + z^2$) and θ the zenith angle with

$$x = r \sin\theta \cos\psi \tag{8}$$

$$y = r \sin\theta \sin\psi \tag{9}$$

$$z = r \cos\theta \tag{10}$$

(see Figure 1b). The polar angle ψ does not enter the solution due to symmetry. The functions R_n and Θ_n are

$$\begin{aligned} R_n(r) &= r^{-0.5}[A_n J_{n+0.5}(\chi r) + B_n Y_{n+0.5}(\chi r)] \\ \Theta_n(\theta) &= C_n P_n(\cos\theta) + D_n Q_n(\cos\theta) \end{aligned} \tag{11}$$

using Bessel functions $J_{n+0.5}$ and $Y_{n+0.5}$, Legendre polynomial P_n and Legendre function Q_n. As χ is an imaginary number and $\cos\theta \leq 1$, consider as a trial solution $H = H^+$ for the outer ($r > r_1$) and $H = H^-$ for the inner ($r < r_1$) region:

$$H^+(r,\theta) = \sum_{n=0}^{\infty} \frac{a_n k_n(0.5\alpha r) P_n(\cos\theta)}{k_n(s)} \tag{12}$$

$$H^-(r,\theta) = \sum_{n=0}^{\infty} \frac{a_n i_n(0.5\alpha r) P_n(\cos\theta)}{i_n(s)} \tag{13}$$

with $s = 0.5\alpha r_1$. The i_n and k_n are modified spherical Bessel functions of the first and third kind defined by [*Abramowitz and Stegun*, 1964, p. 443]:

$$i_n(u) = \left(\frac{\pi}{2u}\right)^{0.5} I_{n+0.5}(u) \tag{14}$$

$$k_n(u) = \left(\frac{\pi}{2u}\right)^{0.5} K_{n+0.5}(u) \tag{15}$$

(for imaginary arguments of $\chi r = -0.5i\alpha r$, Bessel Functions $J_{n+0.5}$ (χr) and $Y_{n+0.5}$ (χr) are constants multiplied by the modified Bessel functions $K_{n+0.5}$ ($0.5\alpha r$) and $I_{n+0.5}$ ($0.5\alpha r$)).

2.1. Evaluation of the Coefficients

[7] Physically, the pressure head h and normal velocities should be continuous at every point along $r = r_1$. Matching pressure head h requires (see equation (4))

$$H^+|_{r=r_1} = H^-|_{r=r_1}$$

The requirement for continuity of the normal velocity at $r = r_1$ is

$$-K_0\left[\frac{\partial\phi}{\partial r} + \alpha(\cos\theta)\phi\right]_{r_1^+} = -K_1\left[\frac{\partial\phi}{\partial r} + \alpha(\cos\theta)\phi\right]_{r_1^-} \tag{16}$$

In terms of the Helmholtz function H, the requirement is

$$\begin{aligned} \left[\frac{\partial H}{\partial r}\right]_{r=r_1^+} - C_1\left[\frac{\partial H}{\partial r}\right]_{r=r_1^-} + 0.5(1 - C_1) \\ \cdot \alpha(\cos\theta)[H + 2\exp(0.5\alpha r)]_{r_1} = 0 \end{aligned} \tag{17}$$

with $C_1 = K_1/K_0$. Note for $C_1 = 0$, the last expression is equivalent to that of *Knight et al.* [1989, equation 8].

[8] Use of equations (12), (13), and (17) leads to

$$\begin{aligned} \sum_{n=0}^{\infty} a_n \left\{\frac{k_n'(s)}{k_n(s)} - C_1\frac{i_n'(s)}{i_n(s)} + (1 - C_1)\cos\theta\right\} P_n(\cos\theta) = 2(C_1 - 1) \\ \cdot (\cos\theta)\exp(s\cos\theta) \end{aligned} \tag{18}$$

The coefficients a_n follow by optimization of equation (18) for multiple choices of θ and using a finite number of terms in the above series. In the solution of *Barnes and Janković* [1999], the continuity of the flux was satisfied exactly whereas the continuity of head was approximate. Here the situation is reversed because it is simpler to match the head and approximate the flux term.

[9] If equation (18) is rewritten using N terms and evaluating at $\theta = \theta_m$, a result convenient for computing a_n follows:

$$\sum_{n=0}^{N} a_n f_{m,n} P_n(\cos\,\theta_m) = g_m \tag{19}$$

with

$$f_{m,n} = -\frac{k_{n+1}(s)}{k_n(s)} - C_1\frac{i_{n+1}(s)}{i_n(s)} + (1 - C_1)\left(\frac{n}{s} + \cos\theta_m\right) \tag{20}$$

$$g_m = 2(C_1 - 1)\,(\cos\theta_m)\exp(s\cos\,\theta_m) \tag{21}$$

In developing equation (20), expressions for the derivative of the modified spherical Bessel functions from *Abramowitz and Stegun* [1964, equation 10.2.21] were used:

$$k_n'(s) = -k_{n+1}(s) + \frac{n}{s}k_n(s) \tag{22}$$

and

$$i_n'(s) = i_{n+1}(s) + \frac{n}{s}i_n(s) \tag{23}$$

[10] Continuing on, by equations (4), (12), and (13) the value of ϕ/ϕ_0 is

$$\frac{\phi}{\phi_0} = 1 + \exp(-0.5\alpha z)\sum_{n=0}^{\infty}\frac{a_n k_n(0.5\alpha r)P_n(\cos\theta)}{k_n(s)}, r > r_1 \tag{24}$$

$$\frac{\phi}{\phi_0} = 1 + \exp(-0.5\alpha z)\sum_{n=0}^{\infty}\frac{a_n i_n(0.5\alpha r)P_n(\cos\theta)}{i_n(s)}, r < r_1 \tag{25}$$

Note that both ϕ and h are continuous across $r = r_1$. The pressure head h is related by

$$\alpha(h - h_0) = \ln\left(\frac{\phi}{\phi_0}\right) \tag{26}$$

2.2. Stokes Stream Function

[11] A Stokes stream function F can be defined for axisymmetrical three-dimensional flow [*Raats*, 1971; *Knight et al.*, 1989]. Conventionally, the value can be taken as zero along the z axis and F to be the flow passing through the horizontal circle defined at z and $\rho = (x^2 + y^2)^{0.5}$:

$$F(\rho, z) = -2\pi\int_0^{\rho} uJ_z|_z du \tag{27}$$

A convenient dimensionless form F_* is

$$F_* = -\frac{F}{\pi r_1^2 J_{z,B}} \tag{28}$$

with $J_{z,B}$ the background flux

$$J_{z,B} = -\alpha K_0\phi_0 \tag{29}$$

(when beyond the influence of the heterogeneous sphere, the dimensionless flux F_* is simply $(\rho/r_1)^2$).

[12] The vertical velocity J_z can be expressed in the form

$$J_z = -K_i\left(\cos\theta\frac{\partial\phi}{\partial r} - \frac{\sin\theta}{r}\frac{\partial\phi}{\partial\theta} + \alpha\phi\right) \tag{30}$$

A corresponding dimensionless form is J_{z*} expressed by

$$J_{z,*} = \frac{J_z}{J_{z,B}} = \frac{K_i}{K_0\phi_0}\left(\frac{\cos\theta}{\alpha}\frac{\partial\phi}{\partial r} - \frac{\sin\theta}{\alpha r}\frac{\partial\phi}{\partial\theta} + \phi\right) \tag{31}$$

leads to the dimensionless stream function

$$F_* = 2\int_0^{\rho/r_1} J_{z*}vdv \tag{32}$$

When J_{z*} is computed from equation (31), useful relations for $r > r_1$ are

$$\frac{1}{\alpha\phi_0}\frac{\partial\phi}{\partial r} = 0.5\left[-\cos\theta\left(\frac{\phi}{\phi_0} - 1\right) + \exp(-0.5\alpha z)\cdot\sum_{n=0}^{N}\frac{a_n k_n'(0.5\alpha r)P_n(\cos\theta)}{k_n(s)}\right] \tag{33}$$

and

$$\frac{1}{\phi_0}\frac{\partial\phi}{\partial\theta} = \sin\theta\left[0.5\alpha r\left(\frac{\phi}{\phi_0} - 1\right) - \exp(-0.5\alpha z)\cdot\sum_{n=0}^{N}\frac{a_n k_n(0.5\alpha r)P_n'(\cos\theta)}{k_n(s)}\right] \tag{34}$$

For similar expressions for $r < r_1$, replace k_n with i_n. The derivative of the zero-order Legendre polynomial is 0; for $n > 0$ the following expression is useful [*Dwight*, 1961, equation 843]:

$$P_n'(u) = \frac{1}{u^2 - 1}[nuP_n(u) - nP_{n-1}(u)] \tag{35}$$

[13] From a practical standpoint, it is expedient to evaluate the stream function from equation (32) directly. (An alternative approach would be to develop an analytical expression for F along the lines of *Knight et al.* [1989, section 1.2].)

3. Results and Examples

[14] As a preliminary step for calculations, the influence of the number of terms N used for truncating the appropriate generalized Fourier series was investigated by the left and right sides of equation (19). If the left and right sides were equal for all choices of θ_m along the surface of the interface, the solution would be exact. In practice, the differences

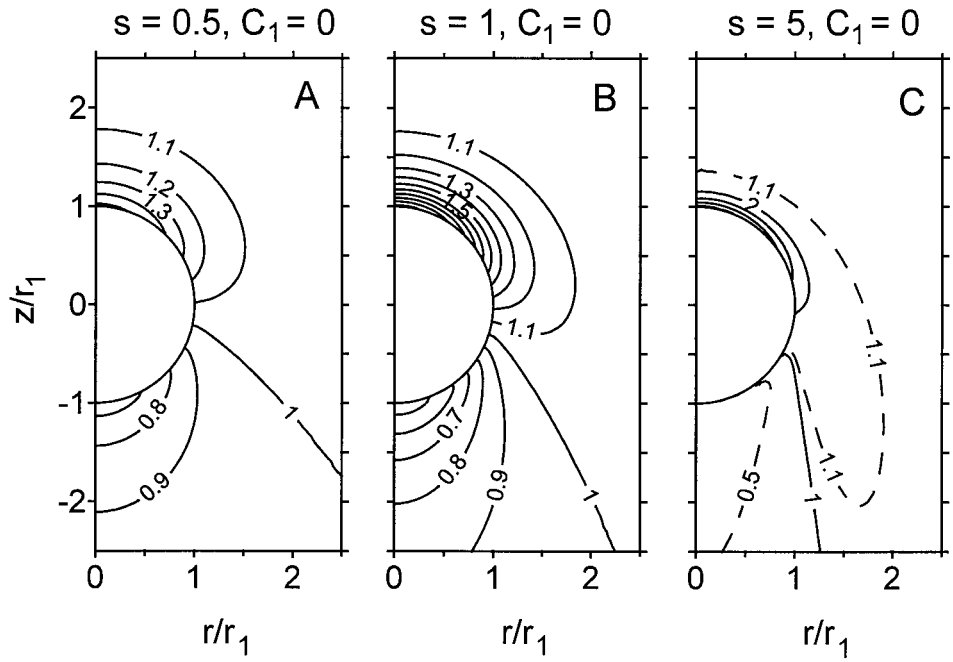

Figure 2. Contours for ϕ/ϕ_o for impermeable inclusions and for (a) $s = 0.5$, (b) $s = 1$, and (c) $s = 5$.

must be acceptably small in some sense. In order to make a meaningful comparison, we define an error term e_m

$$e_m = \frac{(M+1)|s_m - g_m|}{\sum_{m=0}^{M} |s_m|} \tag{36}$$

with s_m given by the left side of equation (19)

$$s_m = \sum_{n=0}^{N} a_n f_{m,n} P_n(\cos \theta_m) \tag{37}$$

Values of a_n were evaluated using the "linfit" function of Mathcad [*Mathsoft*, 1999] to "minimize the sum of the squares of errors." The $M + 1$ values of θ_m were taken equally spaced over 0 to π. Following the principle of "overspecification" [*Janković and Barnes*, 1999], values of M were taken considerably larger than N, usually, 3 or more times larger. Maximum values of e_m were examined for a combination of N values, for varying relative permeabilities $C_1 = K_1/K_0$ (0, 0.5 and 1) and for three contrasting s values (0.5, 1 and 5). For the smallest value of s considered (s = 0.5), the resulting maximum values of e_m were of the order of 10^{-5} for $M = 25$, $N = 5$ and were of the order 10^{-15} for M = 50, $N = 15$. This was true for all of the C_1 values. For $s = 1$, the resulting maximum e_m were larger, on the order of 10^{-3} for $M = 25$, $N = 5$ and 10^{-14} for $M = 50$, $N = 15$. Larger still were the resulting maximum e_m for $s = 5$. These were of the order 10^{-5} and 10^{-6} for $M = 50$, $N = 25$; the results were reduced to 10^{-11} or less with $M = 100$, $N = 25$. Consequently, values of $M = 50$ and $N = 15$ were assumed sufficient and used for the computations which follow. (Values of M could have been increased with essentially no increase in overall computational effort; increases in N result in proportionally larger computational efforts although this was not generally of concern.)

3.1. Flow Around Impermeable Spheres

[15] As a first example, impermeable spheres were considered for s = 0.5, 1 and 5. Values of the Helmholtz function H were determined using equations (12) and (13). The resulting ϕ/ϕ_0 follows by equations (24) and (25). Contours of equal ϕ/ϕ_0 are shown in Figure 2 and may be compared to those of *Knight et al.* [1989, Figure 1]. (Note that the contours of equal ϕ/ϕ_0 are also contours of equal pressure head as related through equation (2)). At large distances from the inclusion, the background flow is constant with a downward Darcian flow rate $K_0 \exp(\alpha h_0)$ corresponding to $\phi/\phi_0 = 1$. The pressure h (and ϕ) increases at the top of the inclusion with a corresponding decrease below. The magnitude of these changes in ϕ/ϕ_0 is shown by the contours above and below the inclusion. For increasing values of s, the patterns of contours change. The changes in values are more gradual with the smaller value of $s = 0.5$ (in Figure 2a) with more extreme gradients for the larger $s = 5$ (in Figure 3c). The extreme changes are more evident in the patterns shown on the leeward side where the minimum contour shown is 0.5 for $s = 5$ and 0.8 for $s = 0.5$. There are two interpretations for the increasing values of s. If the radius of the inclusion is the same, then the physical dimensions of the spheres depicted in Figure 2 are the same, and the increasing values of s is due to decreasing capillary length ($s = 0.5\alpha r_1$ and α is inversely related to capillary length). Figure 2a would correspond to a finer-textured soil, and Figure 2c would correspond to a coarser-textured material. The second interpretation is that the capillary lengths are the same and the hydraulic properties of the soil are the same but the radius of the sphere increases from left to right. In this case, the sphere in Figure 3c would be 10 times larger than that in Figure 3a, and it is easy to

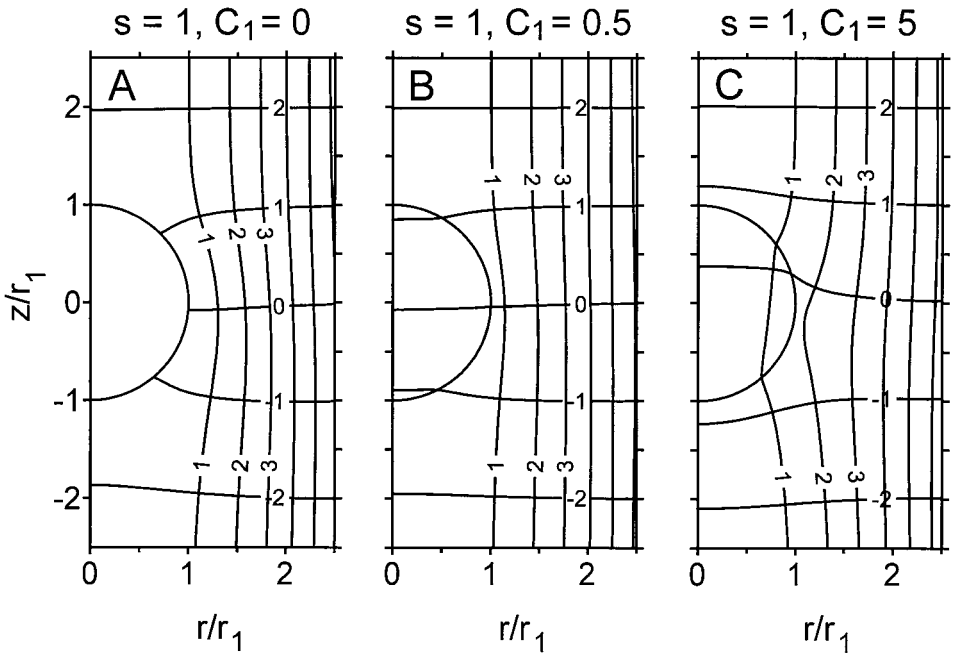

Figure 3. Flow net for s =1 and relative conductivities of (a) 0, (b) 0.5, and (c) 5.

visualize that the pressures are affected more at the sphere and extend much further into the medium. Hence the "1.1" contour in Figure 2c extends far to the right and below, much more so than for the other two cases, particularly in real dimensions.

3.2. Flow Nets Around Spheres of Contrasting Permeability

[16] As a second example, flow nets were prepared for contrasting permeability defined by $C_1 = K_1/K_0 = 0$, 0.5 and 5. Focusing first on the impermeable inclusion (Figure 3a with $C_1 = 0$) note the five curves plotted which extend left to right and labeled 2, 1, 0, −1 and −2. These are lines of dimensionless hydraulic head $(h - h_0 + z)/r_1$. Flow occurs from the greater to lesser values of hydraulic head, that is, from top to bottom due to gravity. At large distances from the inclusion, h approaches h_0 and the hydraulic head reduces to the elevation. The curves orthogonal to the hydraulic head contours tend to be vertical and are labeled to show the dimensionless Stokes stream function from equation (32). The stream function contours show the direction of flow and here show the flow moving around the outside of the sphere. The streamlines divide the profile into volumes (formed by rotating the given streamlines around the z axis) which each carry the same amount of downward flow. The distances between the streamlines becomes increasingly smaller for larger r because the soil volumes are increasing proportionally to r itself.

[17] When the conductivity of the inclusion is finite, flow is diverted away when $C_1 = 0.5$ (Figure 3b) and flows preferentially through the inclusion with $C_1 = 5$ (Figure 3b). This situation can be generalized, flow will be diverted away from an inclusion for $C_1 < 1$ and flow will be enhanced through the inclusion for $C_1 > 1$. A comparison of Figure 3 to similar flow examples for the two-dimensional case [e.g., *Warrick and Knight*, 2002, Figure 4] reveals that the diversion of streamlines is less extreme for the sphere than for the circular inclusion. Table 1 quantifies exclusion and enhancement of from due to the inclusion. For the unsaturated cases, the same three values of $s = 0.5$, 1 and 5 were chosen and the relative flows approximated by the ratio of the streamline values at $r = r_1$, $z = 0$ with and without the inclusion. For example, for $s = 1$ and $C_1 = 0.5$, the relative flow through a sphere is 0.64 compared to the relative flow through a circle for the two-dimensional case of 0.87. Corresponding values for $C_1 = 5$ are 1.35 for the sphere and 1.19 for the circle. For completeness, values are included for the saturated case. The corresponding relationships for the saturated case are F_{3D} for the sphere [*Carslaw and Jaeger*, 1959, p. 426] and F_{2D} for the circle [*Wheatcraft and Winterberg*, 1985, equation 42]:

$$F_{3D} = \frac{3C_1}{2 + C_1} \tag{38}$$

and

$$F_{2D} = \frac{2C_1}{1 + C_1} \tag{39}$$

Note that the fractional flow for the saturated case follows the same trend in that there is a greater exclusion from the sphere for $C_1 < 1$ and a greater enhancement for $C_1 > 1$.

Table 1. Ratios for Streamline Values at $x = r_1$, $z = 0$ With and Without an Inclusion[a]

	$C_1 = 0.5$		$C_1 = 5.0$	
	2D	3D	2D	3D
$s = 0.5$	0.70	0.62	1.57	2.02
$s = 1$	0.74	0.64	1.45	1.85
$s = 5$	0.87	0.78	1.19	1.35
Saturated	0.67	0.60	1.67	2.14

[a]When conductivity is less in the inclusion ($C_1 = K_1/K_0 < 1$), ratios are less than 1; when conductivity is more ($C_1 > 1$), ratios are greater than 1. Results are shown for both 2-D (circular) and 3-D (spherical) inclusions.

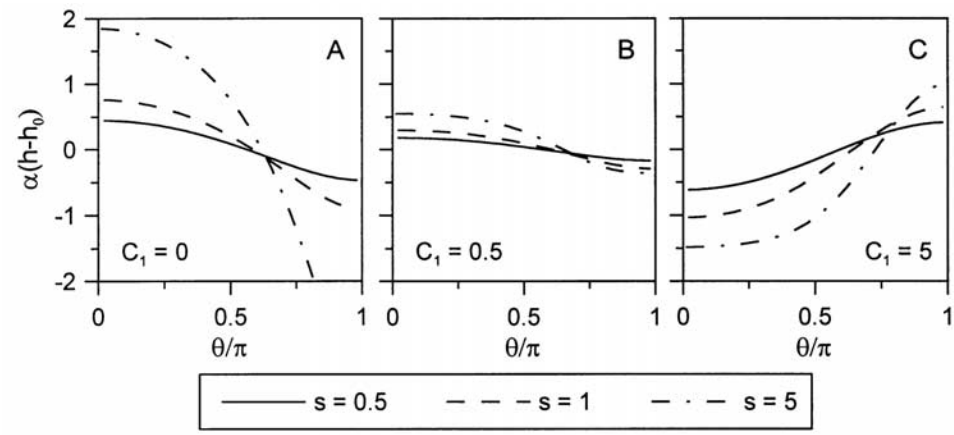

Figure 4. Pressure distributions and spherical interface for (a) $C_1 = 0$, (b) $C_1 = 0.5$, and (c) $C_1 = 5$.

3.3. Pressure Distribution at the Surface of the Spherical Inclusion

[18] The dimensionless pressure α $(h - h_0)$ is given by equation (26). Values of dimensionless pressure are plotted as a function of the fractional polar angle θ/π in Figure 4. When the permeability within the interface is less than the background (Figures 4a and 4b), the pressure is greater than the background at the top (small values of θ/π) and decreases below the inclusion (larger values of θ/π). The more extreme changes are for the largest value of $s = 5$ corresponding to either a greater capillary length or a larger sphere. When the sphere is of higher permeability than the background (Figure 4c), the pressure is less above the sphere and is above the background value below the sphere. For this case the more extreme values are also for the largest s value.

4. Summary and Conclusions

[19] The analytic element method of *Barnes and Janković* [1999] and *Janković and Barnes* [1999] was successfully used to describe unsaturated flow through spherical inclusions. This leads to expressions for potential and flow fields for a permeable inclusion as well as an impermeable inclusion such as that considered by *Knight et al.* [1989]. Generally, computations are easier for smaller values of the dimensionless radius $s = 0.5$ as compared to $s = 5$. For example, 5 terms of the truncated Fourier series give reasonable results for smaller s values whereas 15 were necessary for $s = 5$. Flow exclusion and enhancement through the inclusion were less extreme than for the saturated case. Also, the flow exclusion for low conductivity and flow enhancement for high conductivity were less extreme for spherical inclusions than for circular inclusions. This is consistent with results for the saturated case and is as if the flow paths adjust around or toward the inclusion more easily for the three-dimensional case. As was the case for the two-dimensional case, the pressure decrease is above and pressure increase below the discontinuities when the permeability of the inclusion is higher than that of the background. This is the opposite of what happens for an inclusion with a permeability lower than the background.

[20] Just as for the two-dimensional case, extensions of the approach to include multiple inclusions appear feasible. Also, the detailed flow description should be advantageous over alternative analyses in the development of particle-tracking approaches to study solute dispersion in three-dimensional systems. A drawback of the present analysis is that the capillary length parameter α must be the same in the inclusion as for the background. Current work is in progress to consider the more complex system for which this assumption is not necessary.

[21] **Acknowledgments.** This work was supported, in part, by the National Science Foundation under grant EAR0309515. This research was also supported in part by Western Regional Project W-188.

References

Abramowitz, M., and I. A. Stegun (1964), *Handbook of Mathematical Functions*, *Natl. Bur. Standards Appl. Math. Ser.*, vol. 55, 1046 pp., U.S. Govt. Print. Off., Washington, D. C.

Barnes, R., and I. Janković (1999), Two-dimensional flow through large numbers of circular inhomogeneities, *J. Hydrol.*, *226*, 204–210.

Carslaw, H. S., and J. C. Jaeger (1959), *Conduction of Heat in Solids*, 2nd ed, 510 pp., Oxford Univ. Press, New York.

Dwight, H. B. (1961), *Table of Integrals and Other Mathematical Data*, 4th ed., Macmillan, Old Tappan, N. J.

Gardner, W. R. (1958), Some steady state solutions of the unsaturated moisture flow equation with application to evaporation from a water table, *Soil Sci.*, *85*, 228–232.

Janković, I., and R. Barnes (1999), Three-dimensional flow through large numbers of spheroidal inhomogeneities, *J. Hydrol.*, *226*, 224–233.

Knight, J. H., J. R. Philip, and R. T. Waechter (1989), The seepage exclusion problem for spherical cavities, *Water Resour. Res.*, *25*, 29–37.

Mathsoft (1999), Mathcad user's guide, Cambridge, Mass.

Moon, P., and D. E. Spencer (1961), *Field Theory Handbook*, Springer-Verlag, New York.

Philip, J. R., J. H. Knight, and R. T. Waechter (1989), Unsaturated seepage and subterranean holes: Conspectus, and exclusion problem for circular cylindrical cavities, *Water Resour. Res.*, *25*, 16–28.

Raats, P. A. C. (1971), Steady infiltration from point sources, cavities and basins, *Soil Sci. Soc. Am. Proc.*, *35*, 689–694.

Warrick, A. W., and J. H. Knight (2002), Two-dimensional unsaturated flow through a circular inclusion, *Water Resources Res.*, *38*(7), 1113, doi:10.1029/2001WR001041.

Wheatcraft, S. W., and F. Winterberg (1985), Steady state flow passing through a cylinder of permeability different from the surrounding medium, *Water Resour. Res.*, *21*, 1923–1929.

J. H. Knight, Mathematical Sciences Institute, Australian National University, Canberra, ACT 0200, Australia. (john.knight@maths.anu.edu.au)

A. W. Warrick, Department of Soil, Water, and Environmental Sciences, 429 Shantz Building 38, University of Arizona, Tucson, AZ 85721, USA. (aww@ag.arizona.edu)